Size dependence of the photoinduced magnetism and long-range ordering in Prussian blue analog nanoparticles of rubidium cobalt hexacyanoferrate

Daniel M. Pajerowski and Mark W. Meisel

Department of Physics and the Center of Condensed Matter Sciences, University of Florida, Gainesville, FL 32611-8440, USA

E-mail: dpaj@phys.ufl.edu and meisel@phys.ufl.edu

Franz A. Frye and Daniel R. Talham

Department of Chemistry, University of Florida, Gainesville, FL 32611-7200,USA

E-mail: frye@chem.ufl.edu and talham@chem.ufl.edu

Abstract. Nanoparticles of rubidium cobalt hexacyanoferrate ($Rb_jCo_k[Fe(CN)_6]_l \cdot nH_2O$) were synthesized using different concentrations of polyvinylpyrrolidone (PVP) to produce four different batches of particles with characteristic diameters ranging from 3 to 13 nm. Upon illumination with white light at 5 K, the magnetization of these particles increases. The long-range ferrimagnetic ordering temperatures and the coercive fields evolve with nanoparticle size. At 2 K, particles with diameters less than approximately 10 nm provide a Curie-like magnetic signal.

PACS numbers: 75.75+a, 75.50.Xx, 75.30.Wx, 78.20.Ls, 78.67.Bf

1. Introduction

The investigation of magnetism in the molecule-based solid Prussian blue, $Fe_4[Fe(CN)_6]_3 \cdot xH_2O$, and related analogs has a rich history [1,2], dating back to 1928 [3]. Measurements down to liquid helium temperatures identified the transition to long-range ferromagnetic order [4–6], but an understanding of the magnetic interactions remained elusive until the 1970s, when X-ray [7] and neutron [8] diffraction data identified the crystal structure and the spin delocalization from high-spin Fe(III) to low-spin Fe(II). Interest in these materials was renewed in the 1990s with the synthesis of several mixed-metal Prussian blue analogs with higher magnetic ordering temperatures, along with the 1996 discovery of long-lived photoinduced magnetism in $K_{0.2}Co_{1.4}[Fe(CN)_6] \cdot 6.9H_2O$ [9]. A flurry of experimental and theoretical research has elucidated the fundamental nature of the light-induced effects in three-dimensional bulk materials [10, 11], and recent efforts have been made to integrate the photoinduced magnetism into films [12–18] and

Table 1. A summary of the materials properties of the four sets of samples.

Batch	Starting PVP (g)	Resulting Chemical Formula §	PVP:Co ratio	Diameter (nm)	$T_{c,\mathrm{onset}}^{\mathrm{dark}}$ (K)	$T_{c,\mathrm{onset}}^{\mathrm{light}}$ (K)	H_c^{dark} (G)	H_c^{light} (G)
A	1.0	$Rb_{1.9}Co_4[Fe(CN)_6]_{3.2} \cdot 4.8H_2O$	360	3.3 ± 0.8	< 2	< 2	< 10	< 10
B	0.5	$Rb_{1.8}Co_4[Fe(CN)_6]_{3.2} \cdot 4.8H_2O$	200	6.9 ± 2.5	10	13	~ 15	~ 30
C	0.2	$Rb_{1.7}Co_4[Fe(CN)_6]_{3.2} \cdot 4.8H_2O$	60	9.7 ± 2.1	13	17	250	330
D	0.1	$Rb_{0.9}Co_4[Fe(CN)_6]_{2.9} \cdot 6.6H_2O$	20	13.0 ± 3.2	19	22	1000	1500

nanoparticles, which have technical and biophysical applications. There have been several efforts to synthesize nanoparticles of Prussian blue analogs [19–31], but only a few examples of photoinduced magnetism in these particles have been reported, ‡ including work that isolated $K_jCo_k[Fe(CN)_6]_l \cdot nH_2O$ particles with typical diameters of $8-10$ nm within a silica xerogel [22] and other research producing 11 nm $\times$ 70 nm nanorods of $Mo(CN)_8Cu_2$ protected by polyvinylpyrrolidone (PVP) [26]. In each case, although photoinduced magnetism was observed, the particles did not exhibit long-range order.

The purpose of this paper is to report our ability to synthesize $Rb_jCo_k[Fe(CN)_6]_l \cdot nH_2O$ nanoparticles protected by PVP that exhibit photoinduced magnetism for all sizes and that possess long-range ordering, with coercive fields ranging between $0.25 - 1.5$ kG, in the larger particles. The magnetic properties evolve with size, where at 2 K, the particles with diameters less than approximately 10 nm provide a Curie-like magnetic signal.

2. Synthesis and Characterization

Our $Rb_jCo_k[Fe(CN)_6]_l \cdot nH_2O$ nanoparticles were synthesized by modifying the procedure for Prussian blue nanoparticles described by Uemura and coworkers [23, 24]. A 2 mL solution containing both 28 mg $K_3Fe(CN)_6$ (0.085 mM) and 6.8 mg $RbNO_3$ (0.046 mM) was added dropwise to an 8 mL solution containing 30 mg $Co(NO_3)_2 \cdot 6H_2O$ (0.103 mM) and PVP while stirring rapidly. By varying the amount of PVP (Table 1), the protocol produced samples with different particle sizes and size distributions. After 30 minutes of stirring, the solution was allowed to sit for one week. For transmission electron microscopy (TEM) studies, a 50 μL aliquot of the suspension was diluted 2000 times, and 8 μL of the diluted suspension was placed on a holey carbon grid. A representative image is shown in Fig. 1, and selected area electron diffraction was compared to powder X-ray diffraction patterns to confirm the structure [32]. In addition, infrared spectra

‡ Here, we differentiate photoinduced magnetism, which is used to describe the intrinsic process of the $A_jCo_k[Fe(CN)_6]_l \cdot nH_2O$ Prussian blue analog, from photoswitchable magnetism, which arises from magnetization changes observed upon photoexciting a functionalized component or coating of Prussian blue analog nanoparticles, reported in Refs. 29 and 30.

§ Energy dispersive X-ray spectroscopy (EDS) on similar samples suggests the possibility of trace amounts of K, from the $K_3Fe(CN)_6$ solution, being incorporated as interstitials.

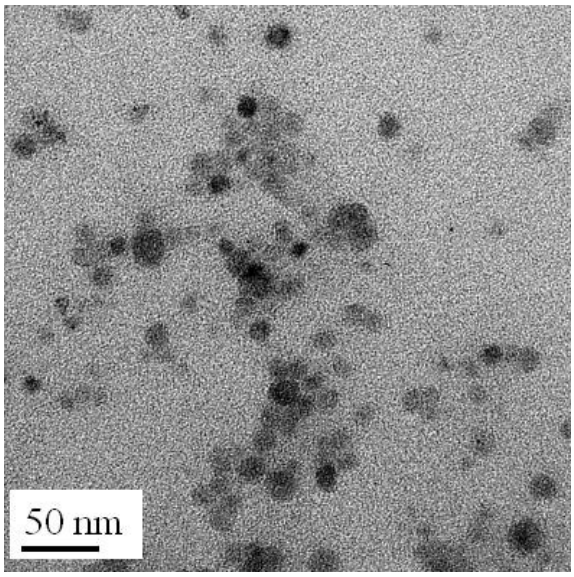

Figure 1. TEM image of a collection of $Rb_{0.9}Co_4[Fe(CN)_6]_{2.9}\cdot(H_2O)_{6.6}$ nanoparticles from Batch D, see Table 1.

displayed a C−N stretch of 2124 cm^{-1}, consistent with a Co(III)−Fe(II) low-spin pair. Using Image J imaging software [33], the TEM images were analyzed to obtain the particle size distributions shown in Fig. 2. ‖ These data were fit to a log-normal function that yielded the characteristic diameters shown in Fig. 2 and Table 1. To isolate the particles, three volumes of acetone were added to the synthesis solution, which was centrifuged, and then further washed with acetone and dried under vacuum. Chemical analysis was obtained from a combination of CHN combustion analysis and inductively coupled plasma mass spectrometry (ICP-MS), and the resulting formulae are listed in Table 1, along with the ratio of the PVP repeat unit per cobalt. The extent of H_2O coordination to the Co was estimated by considering the Fe vacancies implicit with the measured Co:Fe ratio.

3. Photoinduced Magnetism

The temperature dependences of the dc magnetic susceptibilities, $\chi(T) = M/H$, of the four batches of particles are shown in Fig. 3. A standard commercial SQUID magnetometer was employed, and the samples were mounted to commercial transparent tape and could be irradiated with light from a room-temperature, halogen source by using a homemade probe equipped with a bundle of optical fibers [17]. Small diamagnetic background contributions from the holder and tape (representing $\lesssim 0.1\%$ of the total signal) were independently measured and have been subtracted from the data. The magnetic signals are expressed per mole of sample using the chemical formula listed in Table 1. The dark state ZFC data were obtained after cooling in zero applied

‖ Similar size distributions have been obtained for Prussian blue nanoparticles protected by PVP [28].

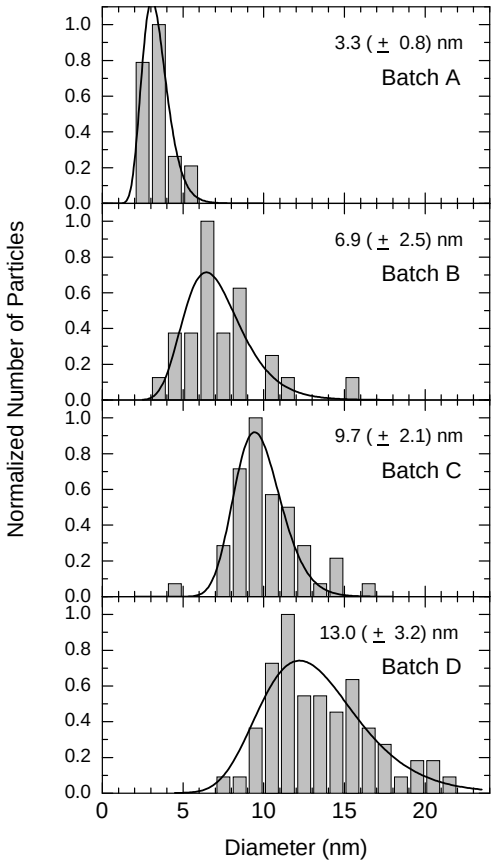

Figure 2. The particle distributions, normalized to the largest bin, versus diameter for the four batches of particles, see Table 1. The total number of particles for each distribution, smallest to largest, is 44, 27, 53, and 62, respectively. The solid lines are the results of log-normal fits that provide the characteristic diameters shown for each distribution.

field from 300 K, while the dark state FC data were taken after cooling in 100 G from 300 K. The light state was established after field cooling the samples from 300 K to 5 K in 100 G and subsequently irradiating with light for 5 hours, which saturated the photoinduced response. In order to avoid spin glass-like relaxation, the light state FC data were obtained after cycling the sample to 30 K in 100 G.

4. Discussion

It is noteworthy to recall that the photoinduced magnetism of the Prussian blue analogs depends upon a charge transfer induced spin crossover event (CTIST effect), requiring the presence of vacancies to allow crystalline flexibility [34–41]. More specifically for $Rb_jCo_k[Fe(CN)_6]_l \cdot nH_2O$, the spins of an Co−Fe pair can exist in either of two arrangements. The low-spin state consists of Co(III) ($S = 0$) and Fe(II) ($S = 0$), while the high-spin state possesses Co(II) ($S = 3/2$) and Fe(III) ($S = 1/2$). The presence of the CTIST effect depends on the local chemical environment defined by the values of j,

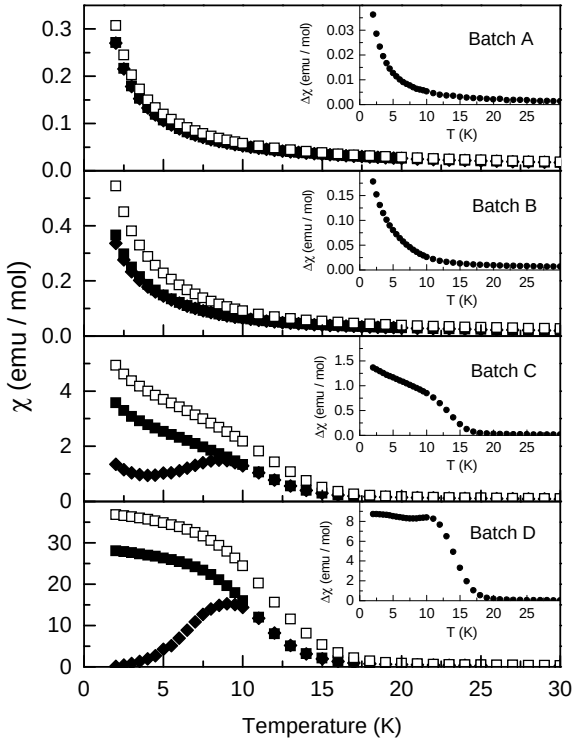

Figure 3. The temperature dependences of the low field, 100 G, susceptibilities are shown for the zero-field cooled (ZFC) dark (♦), field-cooled (FC) dark (■), and FC light (□) states of each batch produced. The insets display the differences between the FC light and dark states, as described in the text. Finite values for this difference can only arise from photoinduced magnetism.

k, l and n in the chemical formula. For limiting ratios, Co and Fe spins can be locked into either their high-spin or low-spin states for all accessible temperatures. Alternatively, with the proper tuning of the chemical ratios, the Co and Fe ions can exist in high-spin states at room temperature and then experience a crossover to their low-spin states at approximately 150 K. The spin crossover phenomenon generates the pairs involved in the photoinduced magnetism. However, since the CTIST effect may not be 100% efficient, some regions remain locked in their high-spin states, and we refer to them as *primordial* spins [13]. For example, these primordial spins are responsible for the magnetic signals observed for the dark state of the largest particles. When irradiated, the low-spin regions, near the primordial high-spin clusters, are photoinduced to the high-spin magnetic state, resulting in a growth of the magnetic domain. This scenario is supported by our description of the anisotropic photoinduced magnetism observed in thin films [13, 18] and by the local probe investigations of others [42, 43]. All samples show a photoinduced increase in their magnetic signals, and the strength of the change is correlated with the size of the particles. The differences between the FC susceptibilities of the light and dark states,

$$\Delta\chi = \chi_{FC}^{light} - \chi_{FC}^{dark} \quad , \tag{1}$$

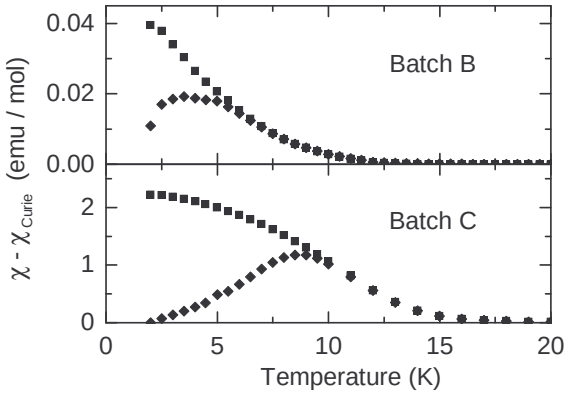

Figure 4. The dark state, i.e. primordial, ZFC (♦) and FC (■) states show a signal associated with long-range order for the two batches displaying a mix of magnetic behavior after subtracting the Curie-like contribution. The susceptibility of Batch A only exhibits a Curie-like contribution, while the magnetic signal for Batch D is dominated by spins that are ordered, see text for details. For each sample, a Curie-like contribution was obtained by fitting the dark state data above 30 K, and this magnetic signal was subtracted from the FC and ZFC dark state data shown in Fig. 3.

are plotted in the insets of Fig. 3, and finite values can only arise from the photoinduced magnetism. It is important to stress that photoinduced magnetism is observed even in small particles possessing only Curie-like behavior.

Two main features are seen when considering the evolution of material properties due to the increasing average size of the separate batches, namely the onset of long-range magnetic order and an increasing net magnetization. This scaling of magnetization is linked to an increased diamagnetic-surface to magnetically-active-volume ratio at smaller particle sizes. At low temperatures, the high-spin Co and Fe ions interact antiferromagnetically, giving rise to a ferrimagnetic transition at T_C, which is about 24 K for bulk powder specimens with a similar chemical formula [36]. For the magnetic data shown in Fig. 3, the onset of this transition can be estimated, and these macroscopic temperatures are listed in Table 1. We contend that particles larger than a critical size will allow domains large enough to approach bulk-like magnetic properties. Conversely, smaller particles may put limits on allowed domain size, suppressing the ordering temperature. Microscopically, if the size of the magnetic domains is less than or of the order of the magnetic coherence length, then a spectrum of T_C values can be expected, and evidence of this trend is observed in Batches C and D, see the insets of Fig. 3. In other words, the size distributions may include particles both above and below the critical size that leads to bulk-like properties. As a result, the magnetic response of each batch may include contributions from Curie-like and bulk-like fractions. The percentage of each can be estimated by subtracting a Curie-like signal from each $\chi(T)$ plot, and the results for Batches B and C are shown in Fig. 4. In contrast, Batch A follows Curie-like behavior, whereas the active sites in Batch D are almost entirely ferrimagnetically ordered. This analysis of the data suggests the Curie-like contribution for each of

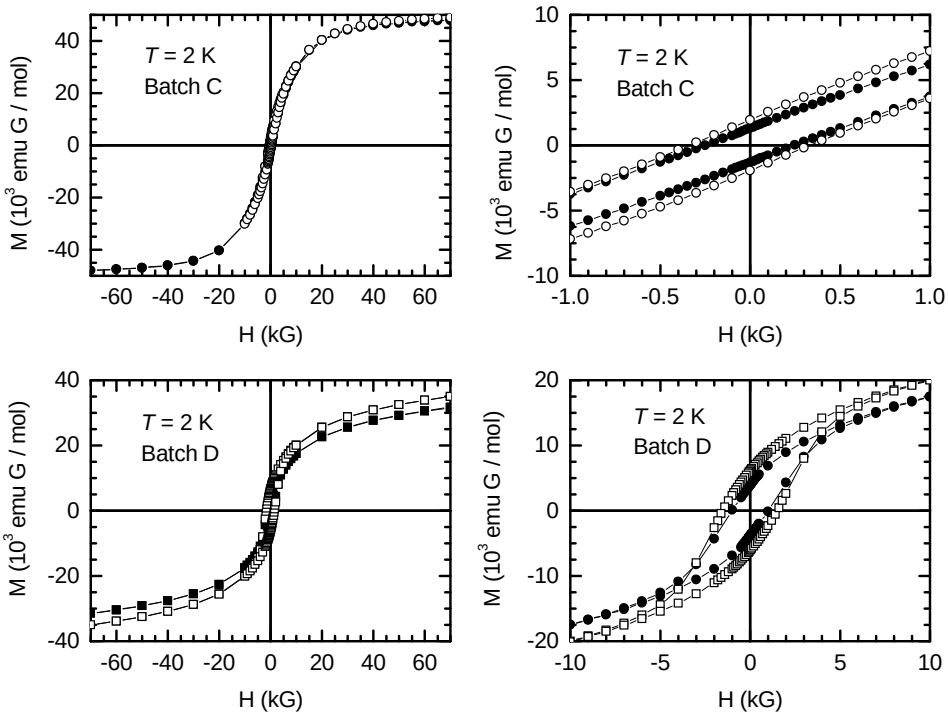

Figure 5. The $T = 2$ K magnetization versus magnetic field sweeps for the two largest sizes of nanoparticles, Batches C and D, are shown for the light (○ and □) and dark (● and ■) states. The coercive fields, H_C for the light and dark states for each batch are listed in Table 1, and the lines are guides for the eyes.

the four batches of nanoparticles (smallest to largest) is 100%, 90%, 50%, and 10%. Consequently, at least down to 2 K, nanoparticles with sizes below $\sim$ 10 nm do not exhibit long-range order. These interpretations are consistent with our M versus H measurements performed at 2 K, where coercive fields, H_C, and remnant magnetization values are observed for the largest sets of particles but not for the smallest set of particles, Fig. 5 and Table 1. Furthermore, the differences between the FC and ZFC data for the dark states in Batches B, C, and D are consistent with spin glass or cluster glass behavior [44, 45], and our ac susceptibility data are presented in the Appendix.

5. Conclusions

In conclusion, we have synthesized four different sizes of $Rb_jCo_k[Fe(CN)_6]l \cdot nH_2O$ nanoparticles protected by PVP. Each batch of particles exhibits photoinduced magnetism, but the strength of this effect, as well as other global properties, e.g. T_C and H_C, are correlated with the intrinsic particle size distributions of each batch. The combination of photoinduced magnetism and nanosized Prussian blue analog particles with finite coercive fields is unique and establishes a length scale limit of $\sim$ 10 nm for these properties. The next advances in the field will undoubtedly employ Prussian blue analogs with higher transition temperatures [46] that may have a variety of

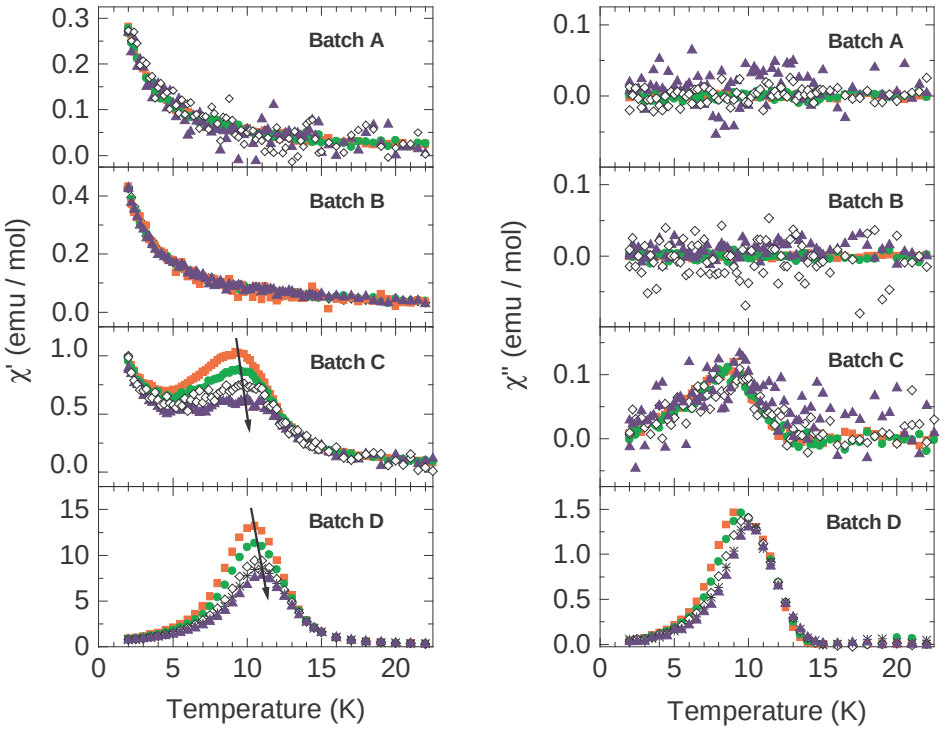

Figure A1. The temperature dependences of the real (χ') and imaginary (χ'') ac susceptibilities of the ZFC dark states, i.e. primordial states, are shown for all four batches of nanoparticles. All batches were measured with no applied static field and an alternating field of 4 G, except for Batch D, which was measured in 1 G. The frequency dependence was studied at 1 Hz (■), 10 Hz (●), 100 Hz (◊), and 1 kHz (▲) for all batches, except for Batch D, which has an additional measurement at 333 Hz (∗). Arrows are guides for the eyes and pass through the peaks.

technical applications, including, for example, the exploitation of optically controlled magnetocaloric properties [47].

Acknowledgments

This work was supported, in part, by NSF DMR-0305371 (MWM) and NSF DMR-0543362 (DRT). We acknowledge early contributions by N. E. Anderson, J. Long and J.-H. Park. We thank the UF Department of Geology for the ICP-MS work and the UF Major Analytical Instrumentation Center for the TEM images.

Appendix

The temperature dependences of the real (χ') and imaginary (χ'') ac susceptibilities of the ZFC dark states, i.e. primordial states, of all four batches are shown in Fig. 6. The

phenomenological parameter, β, given by [44]

$$\beta \;=\; \frac{\Delta T_f}{T_f \Delta(\log \omega)} \quad , \tag{A.1}$$

where T_f is the freezing temperature given by the cusp in $\chi'(T)$ and ω is the angular frequency, is 0.024 ± 0.004 for Batches C and D, and this observation is consistent with spin glass or cluster glass behavior [44, 45].

References

[1] Dunbar K R and Heintz R A 1997 in *Progress in Inorganic Chemistry* Karlin K D ed (New York NY: Wiley and Sons) Vol 45 p 283
[2] Verdaguer M and Girolami G 2004 in *Magnetism: Molecules to Materials V* Miller J S and Drillon M eds (Weinheim: Wiley-VCH) p 284
[3] Davidson D and Welo L A 1928 *J. Phys. Chem.* **32** 1191
[4] Holden A N, Matthias B T, Anderson P W and Lewis H W 1956 *Phys. Rev.* **102** 1463
[5] Bozorth R M, Williams H J and Walsh D E 1956 *Phys. Rev.* **103** 572
[6] Ito A, Suenaga M and Ôno K 1968 *J. Chem. Phys.* **48** 3597
[7] Buser H J, Schwarzenbach D, Petter W and Ludi A 1977 *Inorg. Chem.* **16** 2704
[8] Day P, Herren F, Ludi A, Gudel H U, Hulliger F and Givord D 1980 *Hel. Chim. Acta* **63** 148
[9] Sato O, Iyoda T, Fujishima A and Hashimoto K 1996 *Science* **272** 704
[10] Ohkoshi S and Hashimoto K 2001 *J. Photochem. Photobio. C: Photochem. Rev.* **2** 71
[11] Varret F, Nogues M and Goujon A 2002 in *Magnetism: Molecules to Materials I* Miller J S and Drillon M eds (Weinheim: Wiley-VCH) p 257
[12] Yamamoto T, Umemura Y, Sato O and Einaga Y 2004 *Chem. Lett.* **33** 500
[13] Park J-H, Cižmár E, Meisel M W, Huh Y D, Frye F, Lane S and Talham D R 2004 *Appl. Phys. Lett.* **85** 3797
[14] Yamamoto T, Umemura Y, Sato O and Einaga Y 2004 *Chem. Mater.* **16** 1195
[15] Park J-H, Frye F, Lane S, Cižmár E, Huh Y D, Talham D R and Meisel M W 2004 *Polyhedron* **24** 2355
[16] Yamamoto T, Umemura Y, Sato O and Einaga Y 2005 *J. Am. Chem. Soc.* **127** 16065
[17] Park J-H 2006 *Ph.D. Thesis* (Gainesville, University of Florida)
[18] Frye F A, Pajerowski D M, Lane S M, Anderson N E, Park J-H, Meisel M W and Talham D R 2007 *Polyhedron* **26** 2281
[19] Vaucher S, Li M and Mann S 2000 *Angew. Chem. Int. Ed. Engl.* **39** 1793
[20] Ng C W, Ding J, Chow P Y, Gan L M and Quek C H 2000 *J. Appl. Phys.* **87** 6049
[21] Vaucher S, Fielden J, Li M, Dujardin E and Mann S 2001 *Nano Lett.* **2** 225
[22] Moore J G, Lochner E J, Ramsey C, Dalal N S and Stiegman A E 2003 *Angew. Chem.* **115** 2847
[23] Uemura T and Kitagawa S 2003 *J. Am. Chem. Soc.* **125** 7814
[24] Uemura T, Ohba M and Kitagawa S 2004 *Inorg. Chem.* **43** 7339
[25] Yamada M, Arai M, Kurihara M, Sakamoto M and Miyake M 2004 *J. Am. Chem. Soc.* **126** 9482
[26] Catala L, Mathonière C, Gloter A, Stephan O, Gacoin T, Boilot J-P and Mallah T 2005 *Chem. Commun.* 746
[27] Johansson A, Widenkvist E, Lu J, Boman M and Jansson U 2005 *Nano Lett.* **5** 1603
[28] Xian Yu, Zhou Y, Xian Ya, Zhou L, Wang H and Jin L 2005 *Anal. Chim. Acata* **546** 139
[29] Taguchi M, Yamada K, Suzuki K, Sato O and Einaga Y 2005 *Chem. Mater.* **17** 4554
[30] Taguchi M, Yagi I, Nakagawa M, Iyoda T and Einaga Y 2006 *J. Am. Chem. Soc.* **128** 10978
[31] Catala L, Gloter A, Stephan O, Rogez G and Mallah T 2006 *Chem. Commun.* 1018
[32] Frye F A, Pajerowski D M, Anderson N E, Long J, Park J-H, Meisel M W and Talham D R 2007 *Polyhedron* **26** 2273

[33] Rasband W S ImageJ http://rsb.info.nih.gov/ij/ (accessed October 1, 2006) U.S. National Institutes of Health, Bethesda, Maryland, USA
[34] Yoshizawa K, Mohri F, Nuspl G and Yamabe T 1998 *Phys. Chem.* B **102** 5432
[35] Kawamoto T, Asai Y and Abe S 2001 *Phys. Rev. Lett.* **86** 348
[36] Bleuzen A, Lomenech C, Escax V, Villain F, Varret F, Cartier dit Moulin C and Verdaguer M 2000 *J. Am. Chem. Soc.* **122** 6648 (Independently, we have generated bulk samples with light state $T_C(onset) \approx 24$ K.)
[37] Cartier dit Moulin C, Villain F, Bleuzen A, Arrio M-A, Sainctavit P, Lomenech C, Escax V, Baudelet F, Dartyge E, Gallet J-J and Verdaguer M 2000 *J. Am. Chem. Soc.* **122** 6653
[38] Escax V, Bleuzen A, Cartier dit Moulin C, Villiam F, Goujon A, Varret F and Verdaguer M 2001 *J. Am. Chem. Soc.* **123** 12536
[39] Champion G, Escax V, Cartier dit Moulin C, Bleuzen A, Villian F, Baudelet F, Dartyge E and Verdaguer M 2001 *J. Am. Chem. Soc.* **123** 12544
[40] Shimamoto N, Ohkoshi S, Sato O and Hashimoto K 2002 *Inorg. Chem.* **41** 678
[41] Escax V, Champion G, Arrio M-A, Zacchigna M, Cartier dit Moulin C and Bleuzen A 2005 *Angew. Chem. Int. Ed.* **44** 4798
[42] Hanawa M, Moritomo Y, Kuriki A, Tateishi J, Kato K, Takata M and Sakata M 2003 *J. Phys. Soc. Jpn.* **72** 987
[43] Salman Z, Parolin T J, Chow K H, Keeler T A, Miller R I, Wang D and MacFarlane W A 2006 *Phys. Rev.* B **73** 174427
[44] Mydosh J A 1993 *Spin Glasses: An Experimental Introduction* (London: Taylor and Francis)
[45] Pejakovič D A, Manson J L, Miller J S and Epstein A J 2000 *Phys. Rev. Lett.* **85** 1994
[46] Ruiz E, Rodrìguez-Fortea A, Alvarez S and Verdaguer M 2005 *Chem. Eur. J.* **11** 2135
[47] Manuel E, Evangelisti M, Affronte M, Okubo M, Train C and Verdaguer M 2006 *Phys. Rev.* B **73** 172406